Biohybrid plants with electronic roots via in vivo polymerization of conjugated oligomers

Daniela Parker, Yohann Daguerre, Gwennaël Dufil, Daniele Mantione, Eduardo Solano, Eric Cloutet, Georges Hadziioannou, Torgny Näsholm, Magnus Berggren, Eleni Pavlopoulou, et al.

Biohybrid plants with electronic roots via *in-vivo* polymerization of conjugated oligomers

*Daniela Parker[1], Yohann Daguerre[2], Gwennael Dufil[1], Daniele Mantione[3], Eduardo Solano[4], Eric Cloutet[3], Georges Hadziioannou[3], Torgny Näsholm[2], Magnus Berggren[1,5], Eleni Pavlopoulou[6], Eleni Stavrinidou[1,2,5]***

1)Laboratory of Organic Electronics, Department of Science and Technology, Linköping University, SE-60174, Norrköping, Sweden

2)Umeå Plant Science Centre, Department of Forest Genetics and Plant Physiology, Swedish University of Agricultural Sciences, SE 90183 Umea, Sweden

3)Université de Bordeaux, Bordeaux INP, CNRS, LCPO UMR 5629, F-33615, Pessac, France

4) NCD-SWEET beamline, ALBA Synchrotron Light Source, Carrer de la Llum 2-26, 08290 Cerdanyola del Vallès, Spain

5)Wallenberg Wood Science Center, Linköping University, SE-60174, Norrköping, Sweden

6) Institute of Electronic Structure and Laser, Foundation for Research and Technology—Hellas, P.O. Box 1527, 71110 Heraklion Crete, Greece

email: eleni.stavrinidou@liu.se

* corresponding author

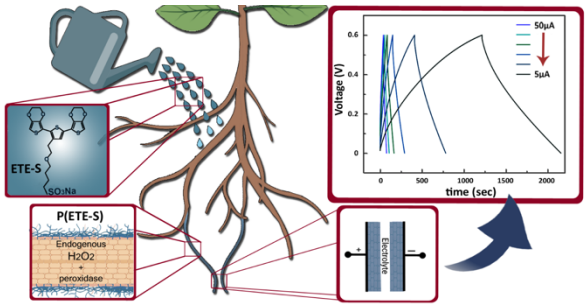

TOC: Conjugated oligomers polymerize in-vivo on the root system of intact plants forming an extended network of tissue integrated conductors while the plants continue to grow and develop. The conducting roots are used to store energy in the plant.

Abstract

Plants processes, ranging from photosynthesis, production of biomaterials to environmental sensing and adaptation can be used in technology via integration of functional materials and devices. Previously, plants with integrated organic electronic devices and circuits distributed in their vascular tissue and organs have been demonstrated. To circumvent biological barriers, and thereby accessing the internal tissue, plant cuttings were used, that resulted in biohybrids with limited lifetime and use. Here we report intact plants with electronic functionality that continue to grow and develop enabling plant-biohybrid systems that maintain fully their biological processes. The biocatalytic machinery of the plants cell wall was leveraged to seamlessly integrate conductors with mixed ionic-electronic conductivity along the plants root system. Cell wall peroxidases catalyzed ETE-S polymerization while the plant tissue served as a template, organizing the polymer in a favorable manner. The conductivity of the resulting p(ETE-S) roots reached the order of 10 S/cm, and it remains stable over the course of 4 weeks while the roots continue to grow. The p(ETE-S) roots were used to build supercapacitors that outperform previous plant-biohybrid charge storage demonstrations. Plants were not affected by the electronic functionalization but adapted to this new hybrid state by developing a more complex root system. Biohybrid plants with electronic roots pave the way for autonomous systems with potential applications in energy, sensing and robotics.

Introduction

Biohybrid technologies aim to merge biological structures and processes with artificial systems to form advanced technological components. A great advantage of biohybrid approaches is that they harness natural processes that have been optimized via millions of years of evolution while biomimetic systems are fully artificial[1, 2]. Over the last decade there has been a growing interest in developing plant-based biohybrid technological systems by integrating smart materials and devices into plant structures[3, 4, 5]. Plants, from a technological perspective, are already amazing machineries. Plants are solar-powered and carbon negative - converting CO_2 to chemical energy, they sense and adapt to various environmental stimuli, and they can self-repair via tissue regeneration. At the same time, they produce several useful materials, with cellulose being the most abundant biopolymer on Earth. Hence, plants offer a broad range of processes that can be leveraged for technological purposes.

In plant nanobionics approaches, for example, smart nanomaterials enable device functionality in plants. The nanoparticles are introduced to the plants where they spontaneously localize within specific plant tissues depending on their size and charge reaching even organelles such as chloroplasts[6,7]. The Strano group developed plant nanobionics environmental sensors for nitroaromatic compounds[8] and arsenite[9] detection. Modified carbon nanotubes infiltrated in the plant leaves produced a readable signal when

the plant up took the analyte of interest from the soil. Nanoparticles were also used as carriers of chemiluminescent reactants within the plant tissue, therefore rendering the plant light emitting[10].

We have merged plants with conjugated polymers and introduced the concept of Electronic Plants where circuits and electrochemical devices are integrated into the plant structure[4, 11]. Conjugated polymers are very promising materials for biohybrid systems as they support mixed ionic-electronic conduction and therefore can act as transducers between biology and electronics[12,13]. Their molecular structure can be tailored to react specifically with biological moieties while being solution processable enables them to take various shapes including free standing form[14,15,16]. By harnessing the physicochemical environment and compartmentalized tissues of the plant we demonstrated that PEDOT polymers can self-organize in the xylem tissue and leaf apoplast and can be used as active layers for transistors and electrochromic pixels respectively[4]. The distribution of the polymers though within the plant was limited close to the side of infusion. Therefore, in a later work we developed a conjugated trimer (ETE-S) that could flow through the plant's vasculature and at the same time polymerize *in vivo* without any external chemical or physical stimuli[11]. Recently we found that cell wall peroxidases, activated by endogenous hydrogen peroxide are responsible for the ETE-S polymerization[17]. Plants therefore have the biocatalytic machinery to polymerize *in vivo* conjugated oligomers and integrate the resulting conducting polymers within their cell walls[17,18]. However, in our previous works we used plant cuttings and not intact plants limiting the lifetime of the biohybrid devices.

In this work, we report electronic functionalization of intact plants via *in vivo* polymerization of conjugated polymers for long term integration of electronics into plants structure. We focused on the plants root system as it responds to various chemical and physical stimuli, regulates the uptake of molecules from the growth environment and secretes numerous organic molecules and therefore is attractive for the development of energy devices and underground sensors [19, 20, 21, 22] .We demonstrate that by simply watering the plant with the conjugated oligomer solution it polymerizes on the roots forming an extended network of easily accessible mixed ionic-electronic conductors while the plant continues to grow and develop.

Results and Discussion

Roots do not have a cuticle and therefore the epidermal cells and cell wall machinery can be directly exposed to conjugated trimers for *in vivo* polymerization. Roots of young bean plants were thus immersed in a freshly prepared aqueous solution of the conjugated trimer ETE-S (1 mg ml^{-1}) (Fig. 1A). The rest of the root system was kept in a nutrient rich solution. Over time we observed a dark coating on the roots indicating polymer formation. The polymerization was confirmed from UV-VIS spectroscopy on roots extracts where the characteristic peak of p(ETE-S) was observed (Fig. S1[11, 23]). To reveal the polymerization kinetics on the roots, we performed time lapse microscopy and monitored *in situ* the polymer formation (Fig S.2). A selection of images is presented in Fig.1B. Within the first 60 min, no significant color change was obvious at the surface of the root indicating very little polymerization. As time went by, the roots became darker with the polymer forming on the epidermal cells; after 300min the root was covered by the polymer. To get further insight on the kinetics we quantified at selected timepoints the root color change corresponding to the polymer amount on the root surface (Fig. S3). The polymer amount increased over time following a sigmodal behavior with initial slow kinetics, then faster kinetics followed by a saturation to 90% (Fig. 1C, Fig. S4). The sigmoidal behavior can be explained by the polymerization mechanism of ETE-S in plants. As previously shown, ETE-S polymerizes enzymatically due to the activity of cell wall peroxidases in presence of endogenous H_2O_2 [17]. Initially, the polymerization is slow because it is limited by the diffusion of ETE-S to the root surface and within the cell walls. When ETE-S molecules react with peroxidases they will oxidize and when two ETE-S radicals combine, dimers will form. Longer oligomers will also form by radical transfer from ETE-S radicals to ETE-S dimers and so on. Therefore, after the initial slow polymerization, faster kinetics were observed with a linear speed of 0.34 % min^{-1} due to the formation of sufficient nucleation sites or ETE-S radicals. At the last phase, we observed saturation of the polymer coating and the half time of the polymerization reaction was found at 152min. Although the polymerization process can continue beyond 350 min, enabling the coating to become thicker, microscopy analysis didn't allow us to picture it as the root became too opaque to observe any further changes in color, explaining the saturation phase.

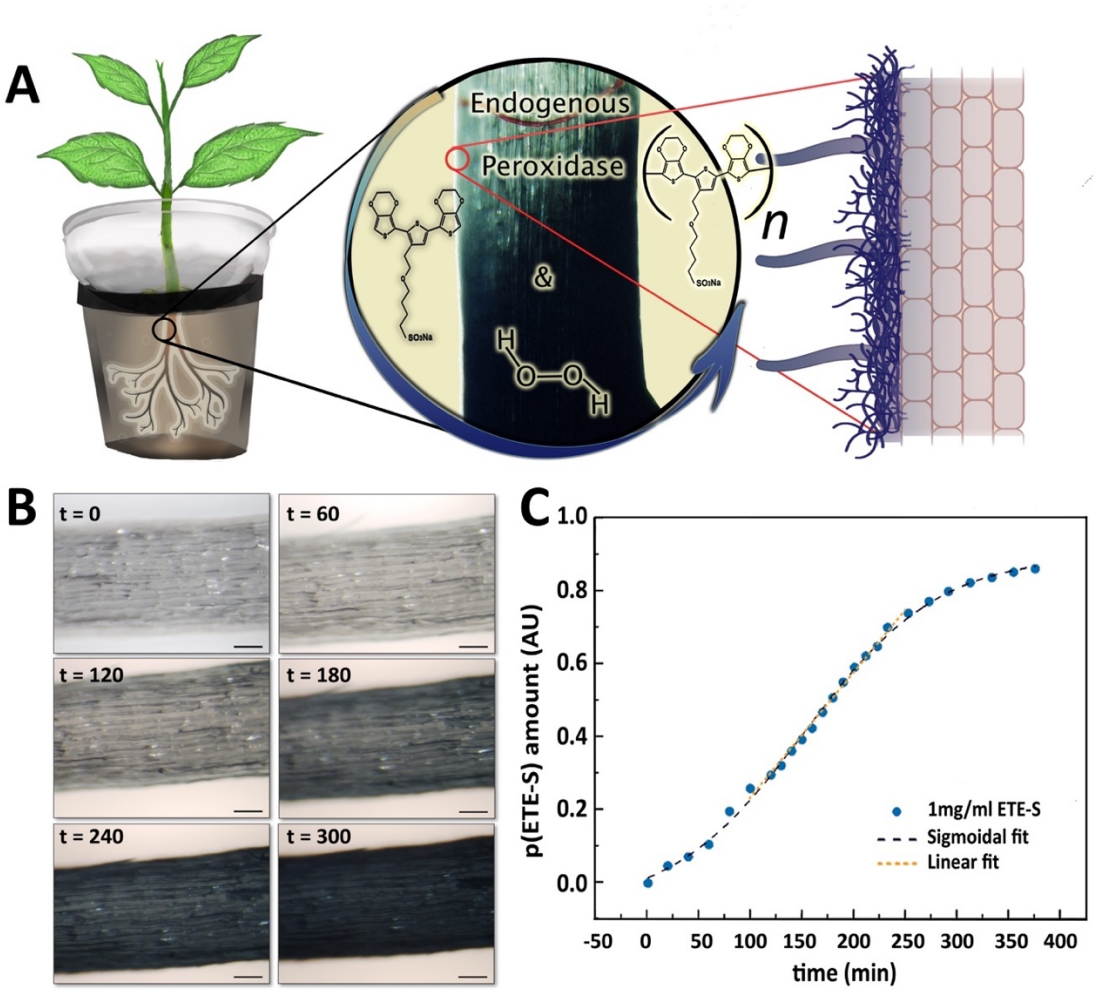

Figure 1: Electronic functionalization of plant roots A) ETE-S polymerizes on the roots of intact bean plant catalyzed by endogenous plant cells wall peroxidases and H_2O_2. B) Micrographs of root during ETE-S polymerization at different times from the onset of the reaction (timescale: minutes, scalebar :100 µm). C) Temporal evolution of p(ETE-S) amount on the root.

After evaluating the initial ETE-S polymerization kinetics on the roots we functionalized the plant for three days and characterized in more detail the polymer localization on the root (Figure 2). Roots are generally sub-divided into three main developmental zones, Fig. 2A [24, 25] .The meristematic area is a site of active cell division from which the root cap or the functional root originate depending on the direction of the division. In the elongation area cells undergo a very rapid elongation, propelling the root through the soil. At this stage the endodermis, casparian strip as well as early vessels elements start to differentiate. In the maturation area, vessels fully differentiate while root hairs and lateral roots might start to appear. In order to study in detail the polymer deposition on the root depending on the

developmental stage, images were taken at different distances from the root tip. Representative plane view images and cross-sections of the meristematic-elongation and the maturation zone are shown in Figure 2 B and C, D respectively. From the plane view images we observed a homogenous and abundant coating along the root, with the exception of the root tip area where the coating was sparse and heterogeneous as exemplified in Fig. 2B. The cross-section images, both longitudinal and transversal, showed that the polymer localized only on the epidermis/exodermis cell layers of the root and this independently of the root developmental stages. Although, as previously demonstrated, internal tissue from plants such as xylem or pith cells have the machinery to polymerize ETE-S[11,17], ETE-S did not reach nor polymerized within the internal structure of intact roots. In some cases, when roots were wounded, we observed polymerization of ETE-S in internal tissue (Fig. S5), but these were isolated observations and never happened with healthy roots. Roots must regulate the uptake of molecules from soil to the vascular tissue in order to ensure proper nutrient exchange and restrict uptake of harmful elements. For this, plants have developed different physiological barriers such as the exodermis and the endodermis. The exodermis is located right below the epidermis and characterized by a Casparian strip, suberin deposition and additional cell wall modification, modulating root permeability depending on its environment [26, 27]. Our results bring evidence that ETE-S do not pass beyond this first barrier. At the root tip, the epidermal/ exodermal cell layers are not yet differentiated, and the root apex is protected by the root cap. A recent study has demonstrated in Arabidopsis that the root cap first cell layer of 2-3 days old seedling possesses a cuticle similar to the one observed in the shoot[28]. However, this protective layer is later replaced by a permanent renewal of the cells, the outer layer being eliminated[29, 30] .In addition, mature root cap secretes a mucilage composed of cell wall polysaccharides and proteins acting as lubricant while the root is prospecting the soil[31, 32]. Such protective mechanisms could explain the heterogeneous deposition of the coating observed in the root tip area and why ETE-S has not entered the internal structure of the root via the root tip. Despite the presence of the coating, the root tissue looked healthy without any obvious damage due to the polymerization such as structural disorganization or deformation of the tissue. From images in Fig. 2D it can be observed that the polymer is forming a coating on the plant cell walls as individual cells acquire a blue coloration (indicated by red arrows). In some cases, the emergence of lateral root is obvious as shown in Fig 2C, D. Next, we investigated if the concentration of ETE-S affected the coating and its localization by functionalizing the plant root with 2 mg ml^{-1} ETE-S (Fig. S6). As before, plant root's main structure was preserved, and the polymer deposited essentially on the epidermis/exodermis cell layers of the root. Root hairs that were present in the maturation zone of these root samples were also coated with the polymer as illustrated in Fig S7. However, some of the coating was detaching from the root and in some cases the epidermal cell layer was peeling off, which could be explained by an increase in the rigidity of the plant cell walls due to a higher deposition and concentration of ETE-S. In the root tip area particularly, the coating is thicker and more granulated than in the case of 1 mg ml^{-1}- ETE-S functionalized roots. At the root cap area, a dense coating is observed even extending beyond

the root tissue reaching the root tip hydrogel (root secretions). Several fully coated cell layers from the root cap were released from the root tip Fig. S6. The renewal of root cap cell layers is a natural process involved in root mucilage secretion and plant response to biotic and abiotic stresses [33]. ETE-S may have triggered an accelerated renewal of this cell layer, however more experiments are needed to test this hypothesis. Overall, the integrity of the root tip and the meristematic area were preserved.

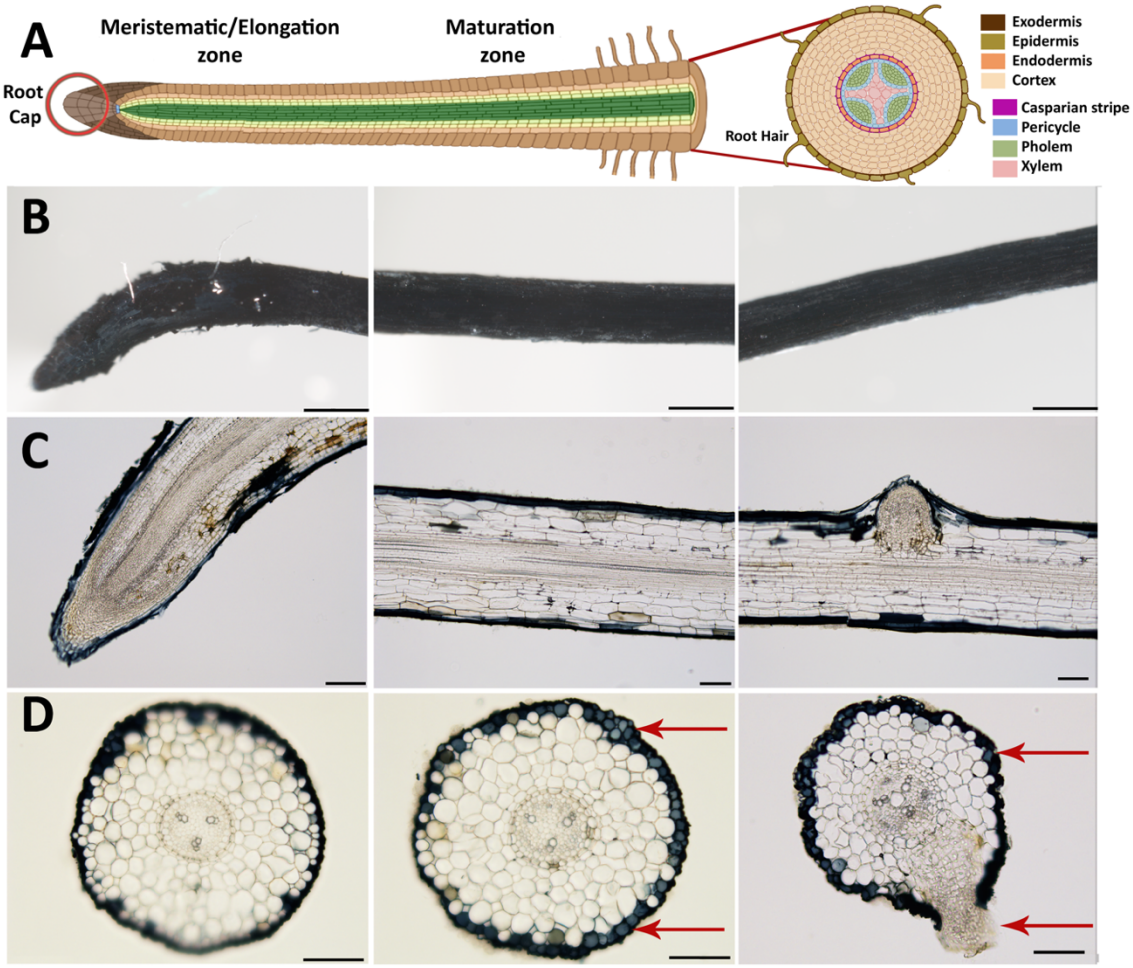

Figure 2: Root functionalized with 1 mg ml^{-1} of ETE-S for 3 days. A) Schematic of root anatomy indicating the various tissues and developmental zones. p(ETE-S) fixed root micrographs for B) plane views (scalebar 500µm) C) longitudinal cross-sections, (scalebar 100µm) and D) transversal cross-sections (scalebar 100µm). In B-D first column corresponds to the meristematic-elongation zone while second and third columns illustrate the maturation zone of the root.

The electrical properties of the roots functionalized with 1 mg ml^{-1} and 2 mg ml^{-1}ETE-S solution were characterized with Current-Voltage (I-V) measurements at various interelectrode distances, Fig. 3A,B. Because of the soft nature of roots and coating we

developed a set up enabling us to probe the functionalized root without applying large pressure nor damaging the coating or the root tissue as described in the methods. The functionalized roots exhibited linear current-voltage dependance without hysteresis and increased resistance with distance which is typical of an ideal resistor behavior. For non-functionalized roots the recorded current was the same as the electrolytic contribution as shown in Fig. S8. To calculate the resistivity, we measured the coating cross section area from the micrographs of the samples characterized. For 1 mg ml^{-1} and 2 mg ml^{-1} ETE-S concentrations, the average areas were 5 * 10^{-5} cm^2 and 5.8 * 10^{-5} cm^2 respectively. We observed an increase in the average area of the coating of the roots functionalized with 2mg ml^{-1} indicating that more material was deposited but not in a linearly proportional manner in agreement with our previous characterization of the fixed samples. Conductivity of the p(ETE-S) was calculated assuming an ideal resistor and was found equal to 12.4 ± 6.1 S/cm and 5.5±1.8 S/cm for roots functionalized with 1 mg ml^{-1} and 2 mg ml^{-1} respectively, Fig. 3C. The conductivity tended to be higher for roots functionalized with 1mg mg ml^{-1} ETE-S but the difference was not significant due to variations among the samples. Next, we evaluated the stability of the conducting layer and how it changed while the functionalized roots were growing. We performed the analysis described above after four weeks from the day of functionalization. During this period the characterized roots remained attached to the plant and the root system was incubated in a nutrient solution. Surprisingly, we did not observe significant changes in conductivity for either of the concentrations. For root functionalized with 1 mg ml^{-1} we observed a small decrease in conductivity while for roots functionalized with 2 mg ml^{-1} a small increase but with no statistical differences in either case. Our results indicate that the p(ETE-S) coating is stable in a nutrient rich solution and retains its conductivity after 4 weeks while the plant is growing. When conducting polymers are used as active materials in bioelectronic devices, they are usually crosslinked prior exposure to biological medium, for better stability[34]. In contrast p(ETE-S) showed strong adhesion to the plant tissue with stable electrical properties without any further processing or additives. We speculated that this was a result of the *in vivo* polymerization and templating of the conducting polymer directly to the plant structure.

To get further insight on the organization and structure of the polymer on the roots, we performed wide-angle x-ray scattering. The patterns recorded for a bare root and a p(ETES)-functionalized root are presented in Figure 3D. The root pattern exhibited a broad peak centered at 1.55 $Å^{-1}$ which was assigned to cellulose[35] and demonstrates its disordered arrangement in the root tissue. After functionalization, a new peak arose at 1.85 $Å^{-1}$, characteristic of the π-π stacking of thiophene rings with a stacking distance of 3.4 Å. This feature was attributed to the organization of the polymerized p(ETE-S) chains along the 010 direction, in consistence with the crystalline structure of PEDOT[36]. This peak was observed for both studied ETE-S concentrations, 1 and 2 mg ml^{-1}. In order to reveal the effect of the root on the organization of p(ETE-S) we enzymatically polymerized ETE-S *in vitro* by mixing ETE-S, horse radish peroxidase and H_2O_2. The obtained polymer solution was then

drop casted on Si substrate. The scattering pattern of this film presented two striking differences with respect to root samples. Intense peaks arose at 0.22, 0.43 and 0.63 $Å^{-1}$, corresponding to the h00 reflections generated by the lamella stacking of polymerized ETES along its aliphatic side chain direction[37]. Such ordering was induced by the confinement of the thin polymeric film on its substrate (herein, silicon).[37] The broad peak observed around 1.65 $Å^{-1}$ was related to the π-π stacking arrangement of the trimers. However, the large width of this peak was characteristic of a lower degree of order, i.e. of a lack of long-range order. Remarkably, this was not the case for *in vivo* polymerized trimer on the root, where the π-π peak was much narrower and centered at a higher q value. This suggested that π-π stacking was more compact with smaller stacking distance. The π-π stacks were better ordered with higher long-range order *in vivo* compared to *in vitro*. This comparison reveals that the plant tissue acts as a template for the polymerization of p(ETE-S) and drives the spatial organization of the polymer, resulting in a better ordering along the π-π direction.

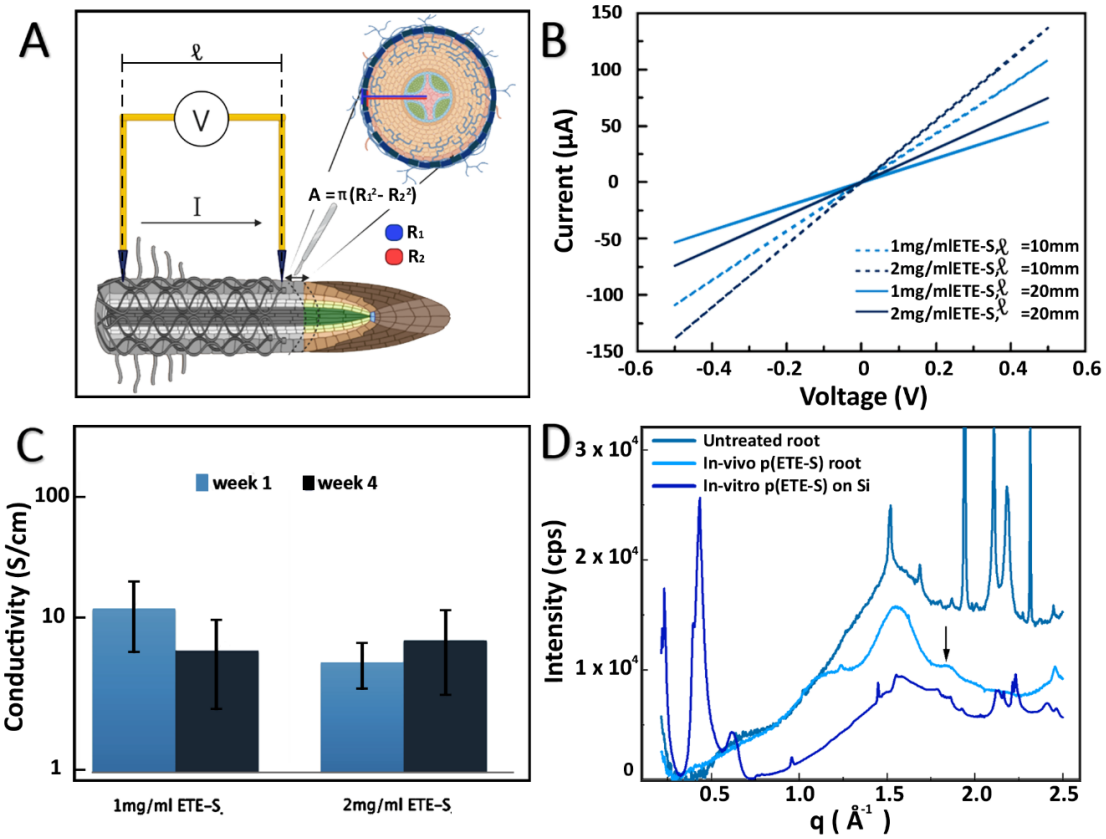

Figure 3: Electrical and structural characterization of p(ETE-S) functionalized roots. A) Schematic of IV measurements and conducting layer cross section determination. B) Current-Voltage curves of p(ETE-S) roots functionalized with 1 or 2 mg/ml ETE-S and for interelectrode distance 10mm and 20mm. C) Average conductivity of p(ETE-S) roots 1 and 4 weeks after functionalization (n=3 for each ETE-S concentration) while they remained attached to the developing plant. D) Scattering profile of control root, p(ETE-S) functionalized root and p(ETE-S) film on Si.

The conductivity measurements showed that ETE-S when polymerized on the roots was conducting and hence doped. The sulfonate side chain acts as a dopant that compensate the positive charges on the polymer backbone making p(ETE-S) a self-doped conjugated polymer [38]. As the sulfonate side chain facilitates the transport of ions, p(ETE-S) is also a mixed conductor capable of transporting both electronic and ionic carriers in a coupled manner. Therefore, p(ETE-S) functionalized roots can be used as active materials in electrochemical devices integrated within the plant. We characterized the electrochemical properties of the roots by cyclic voltammetry (CV). The functionalized root was used as the working electrode in a 3-electrode electrochemical set up with carbon felt as counter electrode and Ag/AgCl as the reference electrode, Fig. 4A. A typical CV curve of ETE-S functionalized root is shown in Figure 4B. We observe that the root was further doped (oxidized) and dedoped (reduced) within a potential window of (-0.5V, +0.5V). The CV had a box shape, ranging between -0.1V and +0.5V, indicating that the doping was based on electrostatic processes and not faradaic; anions from the electrolyte compensated the injected charges on the polymer backbone as in the case of PEDOT [39,23]. At lower potentials the root became resistive as it was being dedoped (reduced). By performing CV in different scan rates, we observed that the current plateau increases linearly with scan rate for 5 and 10mV/s confirming the capacitive nature of the charging. With increasing scan rates, we observed a larger deviation from the box shape. Typically, electrochemical properties of conjugated polymers are assessed by depositing the film on a conducting substrate, so the system is not limited by lateral electronic transport. In the case of p(ETE-S) functionalized root, the electrochemical properties of p(ETE-S) were characterized using the plant root as a substrate which is only ionically conducting. Therefore, the deviation from the box shape at higher scan rates may be a result of ionic or even electronic transport limitation. However, even though electrical contact was made at a single point on the root, our measurements indicated that we could electrochemically address material several mm away from the contact point.

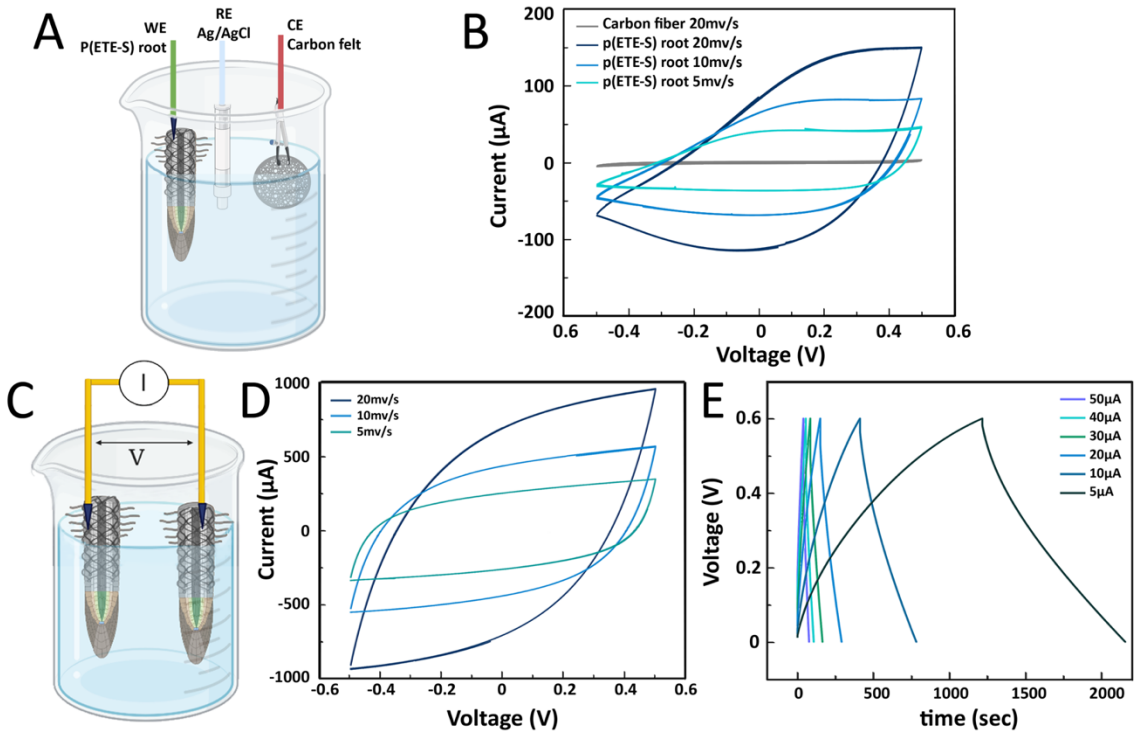

Figure 4: **Electrochemical properties of p(ETE-S) root and root-supercapacitor.** A) Schematic of the 3-electrode set-up used for the cyclic voltammetry of the p(ETE-S) root. B) Typical cyclic voltammogram of p(ETE-S) root at 5,10 and 20mV/s scan rate. C) p(ETE-S) root-supercapacitor schematic D) Cycling voltammogram of the root-supercapacitor at scan rates 5,10 and 20mV s^{-1}. E) Galvanostatic charge-discharge curves at applied currents 5, 10, 20, 30, 40, and 50µA.

Next, we explored the possibility of using the roots for energy storage and built a root-based supercapacitor, Fig. 4C. Supercapacitors based on conducting polymers and cellulose offer an environmentally friendly alternative for energy storage that can be low cost and scalable[40, 41] . Furthermore, there is a growing interest for structural supercapacitors where the volume of an object can contribute to the charge storage[42, 43]. To this end we constructed a proof-of-concept supercapacitor where the roots served as the charge storage electrodes. The cyclic voltammogram had a box shape that deviated from the ideal shape with increasing scan rate as observed in the p(ETE-S) root, indicating limiting ionic or electronic transport[44]. The shape was symmetrical, between +0.5V and -0.5V, signifying that the roots behaved as symmetrical electrodes. To calculate the capacitance of the root-supercapacitor we performed galvanostatic charging- discharging as most supercapacitors are operated in constant current mode. The capacitance was 8mF for the 5µA and decreased with increasing applied current reaching 4mF for 50µA, Table S1. The ESR (Equivalent Series Resistance) was found between 1.3 to 1.8 kΩ, signifying potential drop between p(ETE-S) and electrical contact point. Previously we reported a supercapacitor based on p(ETE-S) wires in the plants' xylem vascular tissue. The typical xylem-supercapacitor had capacitance 0.07mF for 0.5µA,

ESR of 33kOhms and cut-off voltage at 0.25V. In the root-supercapacitor we achieved 100 times higher capacitance with 10 times higher current and with more than double the cut-off voltage. Furthermore, the functionalized roots are readily accessible for external electrical contact, therefore represent a very promising avenue for building energy system integrated in plants.

Plants with integrated conductors for potential use in energy systems or sensing will require not only stability in the electronic components but also that the plant remains healthy after functionalization. Therefore, we characterized the root development and plant growth after functionalization. First, we functionalized the tap root (main root) of young seedlings with ETE-S (Fig. 5). The tap roots were coated with p(ETE-S) and no obvious difference was observed in terms of polymer coating, in comparison with the older roots that were functionalized in the previously discussed experiments (Fig. 1, 2). However, in order to fully investigate if the polymerization efficiency and kinetics depend on the developmental stage of the plant a systematic study is needed that will be the scope of another work. Then we monitored the seedlings growth for 5 days and we observed that p(ETE-S) functionalized tap roots grew more than the tap roots in control plants. The trend was clear but not statistically significant due to large sample variability (Fig. 5C). Therefore, even though the root was covered in polymer, root growth was not inhibited but enhanced. Furthermore, the number of lateral roots emerging from the tap root increased significantly in p(ETE-S) roots after 5 days of growth, extending considerably the complexity of the functionalized root system compared to control plants (Fig. 5D). The enhancement of root growth and lateral root emergence can be a result of an adaptation and compensation of the plant to the polymer-coated tissue. It has been reported that modification of cell walls mechanical properties via Si application increases primary root length and lateral root number[45]. Plant cell wall macromolecules such as lignin, cellulose and pectin seem to template Si deposition in the form of silica even though the molecular mechanisms remain unclear[46]. In the case of ETE-S more biological studies are required to elucidate if ETE-S is altering the mechanical properties of the cell wall or if any other effect on the roots is responsible for the growth enhancement.

As a proof of concept, we also functionalized the whole root system of a plant and followed its growth for 1 month, Fig. 6. We observed that the roots continued to grow and developed new lateral roots. The shoot not only grew bigger but also produced beans. Similar observations were made in the plants where 1 or 2 roots were functionalized for electrical conductivity measurements. Finally, in order to demonstrate that the polymerization of ETE-S is not specific to bean plants root system we also functionalized roots of a pea plant. ETE-S polymerized along the pea plant roots forming a polymer coating (Fig. S9).

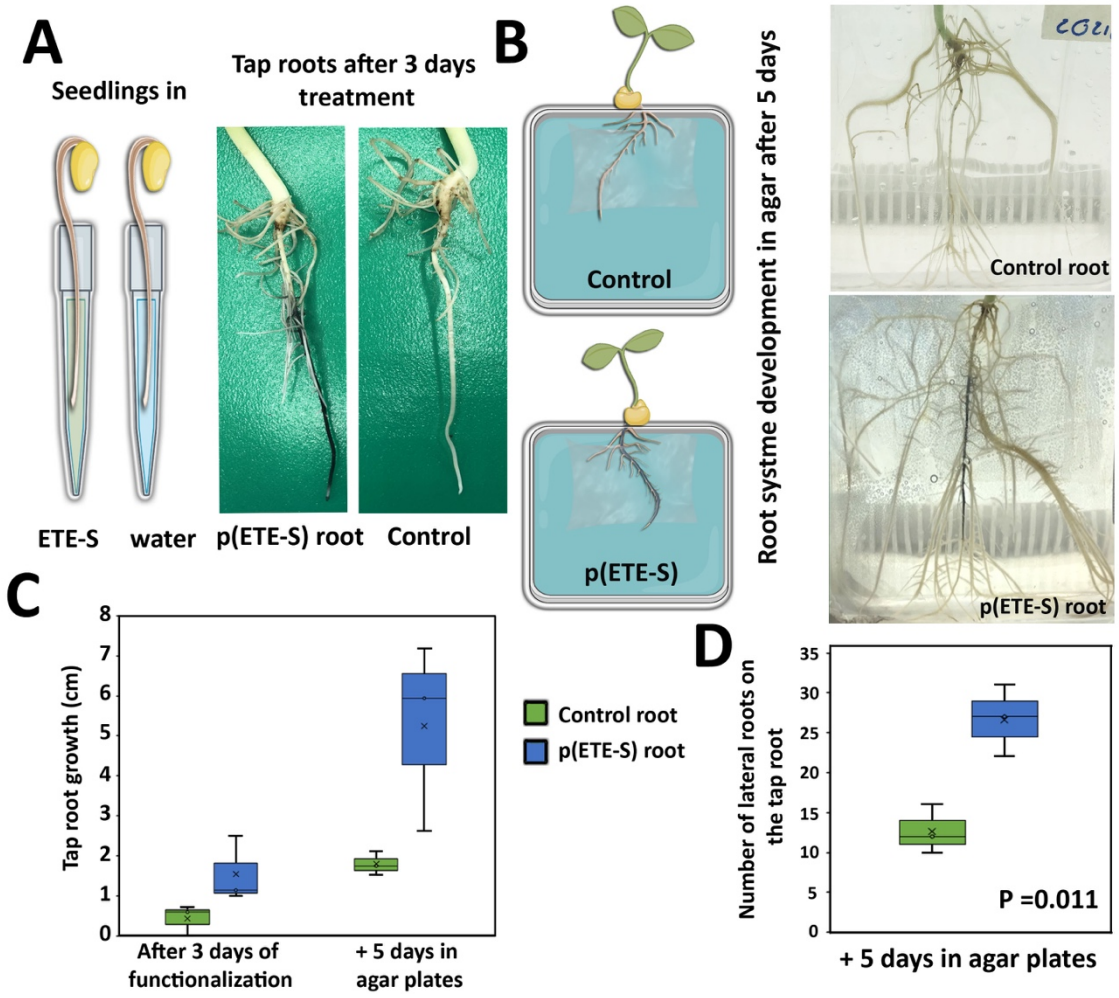

Figure 5: Seedling development after ETE-S functionalization. A) Seedlings were placed in ETE-S solution or water (control) for 3 days. Photographs show the root system after treatment. B) Control and p(ETE-S) seedlings were then placed in agar plates and let grow for 5 days as shown in the photographs. C) Tap root growth in control and p(ETE-S) plants right after functionalization and after 5 days of growth in agar plates. D) Number of lateral roots emerging from tap root after 5 days of growth in agar plates for control and p(ETE-S) plants. (n=3 control, n=3 p(ETE-S) plants, T-test, $P < 0.05$).

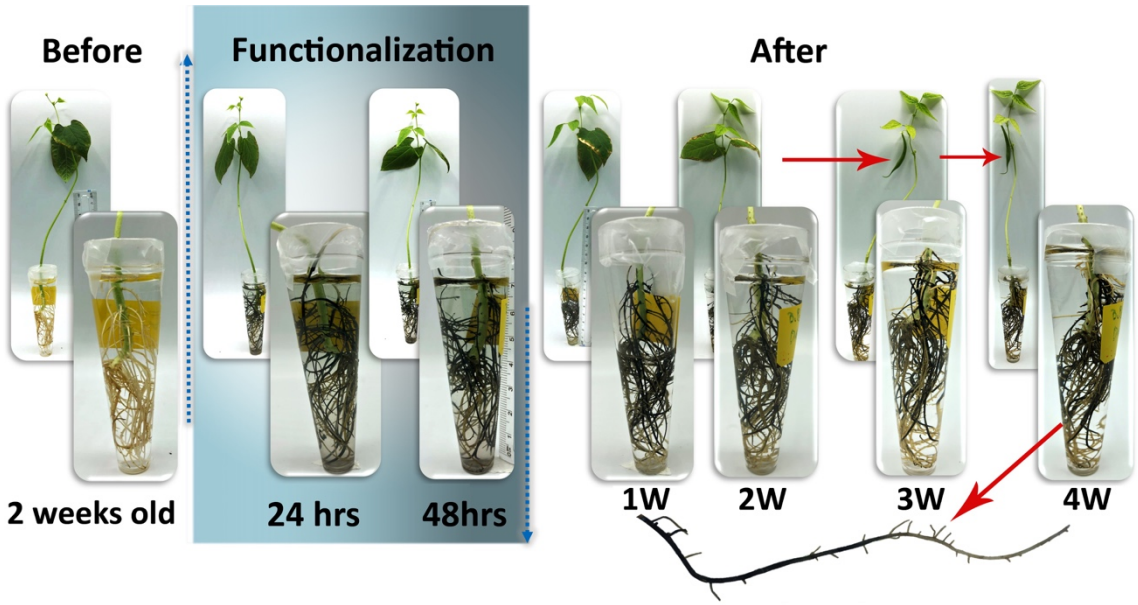

Figure 6: Bean plant growth when whole root system is functionalized with ETE-S. Photographs of the bean plant before, during and after functionalization with ETE-S. At week 3 bean pods are visible in the plant. The individual root close-up shows that new root has grown after the p(ETE-S) coated area.

In conclusion we demonstrated biohybrid plants with an electronic root system. ETE-S in-vivo polymerizes, and the resulting polymer integrates in the epidermal plant cells wall. The p(ETE-S) is structurally templated by the plant tissue, with enhanced pi-pi stacking resulting in a stable conducting coating. The conductivity of the p(ETE-S) roots reaches10S/cm and it is not affected by the plant growth and development for the period of the study, 1 month. Functionalized seedlings developed a more complex root system than control plants indicating the ability of the plant to adapt to the hybrid state. As a proof of concept, we developed a root-supercapacitor with capacitance reaching 8mF and 0.6V cut off voltage outperforming devices previously integrated in the vascular tissue of plant cuttings. Our results overall show that the plant's root system is very promising for functionalization with electronic materials for several reasons. First the lack of cuticle enables the direct exposure of the cell wall biocatalytic machinery to oligomers that are then polymerized into functional components in the tissue in a simple and scalable manner. Secondly the roots are readily accessible for external electrical contact required for addressing and readout. Finally, the root biological functions, from environmental responsiveness to exudation and symbiosis with microorganisms opens a broad range of potential applications for biohybrid systems. In the future we envision biohybrid plants for autonomous energy systems, underground adaptable sensors, and soft robotics.

Methods

Plant growth

Seeds (*Phaseolus vulgaris)* were bought from Impecta Fröhandel and germinated in commercial plant starter cubes Root Riot. Under a laminar flow hood, the cubes were moistened with DI water and the seeds positioned in a small hole in the middle of the cube. Then the scaffold was placed in a closed transparent plastic container sealed with parafilm for five to seven days. The seeds were incubated in the dark at 20-22°C until germination. After germination, seedlings were moved to containers filled with nutrient solution (0.5% v/v in tap water, Hyponex) and placed in the greenhouse with the following growth conditions: temperature 23-25 °C, humidity 50-60%, 12-hours day with a light intensity of 80 -100 μmol m^{-2} s^{-1}.

ETE-S synthesis

ETE-S was synthetized accordingly to the literature[18]. Briefly, a 2,5-dibromination with N-Bromosuccinimide on 3-Thiopheneethanol gave the starting material for a Suzuki reaction using two equivalents of a 2-borolane-EDOT derivate. Then a propane sultone ring-opening give the sulfonate derivate.

Plant root functionalization with ETE-S

Individual roots

Roots from 2-week-old seedlings were functionalized using 1 mg ml^{-1} or 2 mg ml^{-1} of freshly prepared ETE-S aqueous solutions. Roots, about 10-15mm long, were selected after optical inspection to ensure that no wounds were present. While being still attached to the plant, they were placed within an Eppendorf tube containing the ETE-S solution for 72hours. The rest of the root system was kept in the nutrient solution (0.5% v/v in tap water, Hyponex). After functionalization, roots were removed from the ETE-S solution and were placed in the nutrient solution until further characterization.

Whole root system

The whole root system of a two weeks and a half old bean plant was placed in 0.2 mg ml^{-1} ETE-S solution in a 25 ml volume glass container for three days. Afterwards it was placed in a 50ml volume plastic container with tap water to let the plant develop. Photographs of the root system and the whole plant were taken every week for one month.

Time lapse microscopy experiment and image processing

The root from a young plant was immobilized in a reservoir filled with water under a microscope, while the other roots were placed in a commercial gel with nutrients (Seedhru. gel) to avoid dehydration (Fig S2). An initial image was acquired to define the control frame that corresponds to t=0. Afterwards the reservoir was emptied and filled with fresh ETE-S trimer solution of 1 mg ml^{-1} while images were acquired periodically for 300min. The first

two hours and a half, images were taken every 30 seconds. Afterwards images were taken every five minutes until reaching 399 minutes. We converted selected micrographs to gray scale where 0 corresponds to black and 255 to white color (Fig. S3). Within a defined region of interest (ROI), we then calculated the average grey value using Image-J and normalized it to the value at t=0.

Microscopy

Functionalized roots (n=3 for 1 mg $ml^{-1}$and n=2 for 2 mg ml^{-1})were detached from the plant with a sterile scalpel and fixed with paraformaldehyde (PFA) 4% (w/v, dissolved in PBS 1X) at 4°C for 24-48h. At the beginning of the fixation, samples were incubated 1h under vacuum to enhance the penetration of the fixative. After the fixation, the PFA was discarded, and the samples were rinsed twice with PBS 1X and twice with MilliQ water to remove the remaining PFA. Before being further processed, roots were placed on a slide with enough PBS 1X to prevent them from drying out and the deposition of the polymerized ETE-S was analyzed on the root epidermis surface. Images of the surface of the root were taken using a stereomicroscope Leica M205 FA combined with a camera Leica DMC6200 and the objective PLANAPO 2.0x. To make the transversal and longitudinal, root samples were embedded in 4-5% agarose (w/v, dissolved in MilliQ water). For each root area the first half cm was used for longitudinal sections while the second half cm was used for transversal sections. Then, transversal and longitudinal sections, 25µm thick, were taken using a Leica VT1000 S vibratome (Speed 2:75µm/s, Frequency 4:40hz). Following sectioning, sections were mounted in 50% glycerol solution and the slide were closed using nail polish to insure longer preservation. Images were taken using a microscope Leica DMi 8 combined with a camera Leica DFC7000 T and the objectives 10x and 20x.

Electrical conductivity characterization

For the characterization we developed a 3D printed holder with a central channel for the root and perpendicular channels for carbon fibers. The root, while attached to the plant, was placed in the central channel with deionized water to prevent dehydration. Two carbon fibers were placed perpendicular to the root separated by 5, 10, 15 and 20 mm and were used as contact electrodes for the roots. The carbon fibers were addressed via micromanipulators under the microscope with Au-plated tungsten probes (50µm) coated with carbon paste. IV measurements were performed at various lengths with voltage swept between -0.5 to 0.5 V with 0.62 mV s^{-1} scan rate with Keithley K2600B using a custom-made Lab-view program. Assuming an ideal resistor behavior, we plotted the Resistance values versus length and performed a linear fit to extract the R/length for the two ETE-S concentrations, with n=3 for each concentration in week one and week four after functionalization. At the end of the last measurement, transversal sections of the roots were done around the maturation zone to measure the thickness of the coating using a stereomicroscope. To minimize error for each

sample we measured the diameter of the whole root section (D_1) and then diameter of the non-coated area (D_2) in 20 locations. Then the cross-section area of the conductor was calculated $A=\pi(R_1^2-R_2^2)$, and then the conductivity was then calculated from $\sigma = l/(R*A)$.

Electrochemical characterization

Cyclic voltammetry was performed in a three-electrode set-up consisted of the functionalized root as the working electrode, carbon felt (6cm diameter, 2cm thick) as counter electrode, and the Ag/AgCl as the reference electrode. CV with scan rates between 5-20mV s^{-1} and within (-0.5, +0.5 V) were performed in 0.01M KCl electrolyte using Garmy potentiostat 1010B.

Root supercapacitor device fabrication and characterization.

The electrodes of a supercapacitor were defined by two functionalized roots. The spacer of the supercapacitor was defined by the surrounding KCl 0.01M electrolyte. Contact with the electrodes was made using carbon fibers as described in the conductivity measurements. The supercapacitor was characterized by CV and Galvanostatic charging/discharging where the absolute value of charging currents was kept equal to the discharging one. Devices were switched from charging to discharging as soon as the set maximum voltage (0.6 V) was reached. A simple equivalent circuit of R,C in series was used to fit the discharging response of the supercapacitor. The resistor represents the equivalent series resistance.

The device capacitance C, the ESR were extracted using the following relations:
$C= I(dV/dt)$ where I is the applied current, and $dV=dt$ is the slope of the discharge curve as done in standardized characterization of supercapacitors (IEC 62576).
$ESR =\Delta V/2I$, where I is the applied current and ΔV the sudden voltage drop at the beginning of the discharging curve.

ETE-S in-vitro enzymatic polymerization

Enzymatically synthesized p(ETE-S) was obtained by mixing 10 Units ml^{-1} of Horseradish peroxidase with 5 mM of ETE-S, and H2O. The solution was then continuously stirred for 5 min under vortex, letting the time for the total amount of ETE-S to be consumed. The resulting dispersion of polymer was then drop casted on top of a Si substrate and let to dry overnight.

X-ray scattering experiments

Wide-angle x-ray scattering experiments at the transmission geometry and at the grazing incidence geometry (WAXS and GIWAXS, respectively) were performed at the NCD-SWEET beamline of the ALBA Synchrotron, located in Cerdanyola del Vallès, Spain. The wavelength of the X-rays, λ, was 0.9998 Å (12.4 keV), the sample-to-detector distance was

22.91 cm and, in case of the in vitro polymerized films, the angle of incidence, α_i, was set at 0.16°. The diffracted intensity was recorded using a Rayonix LX255-HS detector, which consists of a pixel array of 1920 × 5760 (H × V) and a pixel size of 44 × 44 μm^2. Data were normalized by the incident photon flux and the acquisition time. Flat field, polarization, solid angle and efficiency corrections were additionally applied to the 2D GIWAXS images. The scattering vector q was defined with respect to the center of the incident beam and has a magnitude of $q=(4\pi/\lambda)\sin(\theta)$, where 2θ is the Bragg reflection angle. An azimuthal integration has been performed on the 2D images to obtain the corresponding 1D scattering patterns. 1D scattering patterns are presented herein after background subtraction.

Plant growth assay

Bean seeds were germinated as described in "Plant Growth" section of the methods. After germination the scaffold was removed. The tap root of three seedling was kept in a reservoir with ETE-S fresh solution (1mg ml^{-1} ETE-S), while the rest of the root system was kept in tap water. For the control, the tap root of three seedling, was placed in a reservoir with deionized water, and the rest of the root system was kept in tap water. After three days of functionalization, the root system was washed in Di-W. The seedlings were transferred to agar plates: petri dishes with agar (10g/l) and ½ MS medium were prepared and perforated so that the root system grows in closed conditions while the stem grows in ambient conditions. The seedlings were placed between treated cellophane sheets, and the petri dishes were well sealed with parafilm. Photographs of the root system were taken every day to monitor its growth.

Conflicts of interest

There are no conflicts of interest to declare

Acknowledgements

The authors wish to thank Roger Gabrielsson (Linköping University) for synthesis of ETE-S at the early stages of the study, Jesper Edberg (RISE, Sweden) for fruitful insight on the supercapacitor development and Johannes Gladisch (Linköping University) for help with the 3D-printed conductivity holder. GIWAXS experiments were performed at BL11-NCD-SWEET beamline at ALBA Synchrotron with the collaboration of ALBA staff. Schematics in Figures 2A, 3A, 4A, 4C and 5A, B were created with biorender.com. This work was supported by the European Union's Horizon 2020 research and innovation program under grant agreement No 800926 (FET-OPEN-HyPhOE) and by the Swedish Research Council (VR-2017-04910). Additional funding was provided by European Union's Horizon 2020 Marie Skłodowska-Curie fellowship under grant agreement No 838171 (TEXTHIOL), the Knut and Alice Wallenberg Foundation, the Wallenberg Wood Science Center (KAW 2018.0452), the Swedish Government Strategic Research Area in Materials Science on

Advanced Functional Materials at Linköping University (Faculty Grant SFO-Mat-LiU No. 2009-00971) and the European Research Council (ERC) project e-NeuroPharma 834677.

Author contributions

ES conceived the project, designed, and supervised the research. DP performed most experiments and data analysis including functionalization of roots, all electrical and electrochemical measurements, microscopy, plant growth assay. YD prepared and performed microscopy of fixed samples and assisted in plant biology protocols. GD performed UV-ViS absorption spectroscopy in untreated and treated freeze-dried samples and prepared samples for X-rays analysis. DM synthesized ETE-S. EP performed X-rays scattering experiments and analysis with the help of ESol. MB, TN, EC and GH contributed to the supervision. ES wrote the paper with input from DP, YD, EP and comments from all authors.

References

1 P. Fratzl, *J. R. Soc. Interface*, 2007, 4, 637–642.

2 Y. Liu, K. He, G. Chen, W. R. Leow and X. Chen, *Chem. Rev.*, 2017, 117, 12893–12941.

3 T. T. S. Lew, V. B. Koman, P. Gordiichuk, M. Park and M. S. Strano, *Adv. Mater. Technol.*, , DOI:10.1002/admt.201900657.

4 E. Stavrinidou, R. Gabrielsson, E. Gomez, X. Crispin, O. Nilsson, D. T. Simon and M. Berggren, *Sci. Adv.*, , DOI:10.1126/sciadv.1501136.

5 F. Meder, M. Thielen, A. Mondini, T. Speck and B. Mazzolai, *Energy Technol.*, , DOI:10.1002/ente.202000236.

6 M. H. Wong, R. P. Misra, J. P. Giraldo, S. Y. Kwak, Y. Son, M. P. Landry, J. W. Swan, D. Blankschtein and M. S. Strano, *Nano Lett.*, 2016, **16**, 1161–1172.

7 T. T. S. Lew, M. H. Wong, S. Y. Kwak, R. Sinclair, V. B. Koman and M. S. Strano, *Small*, , DOI:10.1002/smll.201802086.

8 M. H. Wong, J. P. Giraldo, S. Y. Kwak, V. B. Koman, R. Sinclair, T. T. S. Lew, G. Bisker, P. Liu and M. S. Strano, *Nat. Mater.*, 2017, **16**, 264–272.

9 T. T. S. Lew, M. Park, J. Cui and M. S. Strano, *Adv. Mater.*, , DOI:10.1002/adma.202005683.

10 S. Y. Kwak, J. P. Giraldo, M. H. Wong, V. B. Koman, T. T. S. Lew, J. Ell, M. C. Weidman, R. M. Sinclair, M. P. Landry, W. A. Tisdale and M. S. Strano, *Nano Lett.*, 2017, **17**, 7951–7961.

11 E. Stavrinidou, R. Gabrielsson, K. P. R. Nilsson, S. K. Singh, J. F. Franco-Gonzalez,

A. V. Volkov, M. P. Jonsson, A. Grimoldi, M. Elgland, I. V. Zozoulenko, D. T. Simon and M. Berggren, *Proc. Natl. Acad. Sci. U. S. A.*, 2017, **114**, 2807–2812.

12 B. D. Paulsen, K. Tybrandt, E. Stavrinidou and J. Rivnay, *Nat. Mater.*, 2020, 19, 13–26.

13 E. Stavrinidou, P. Leleux, H. Rajaona, D. Khodagholy, J. Rivnay, M. Lindau, S. Sanaur and G. G. Malliaras, *Adv. Mater.*, 2013, **25**, 4488–4493.

14 R. B. Bazaco, R. Gómez, C. Seoane, P. Bäuerle and J. L. Segura, *Tetrahedron Lett.*, 2009, **50**, 4154–4157.

15 D. Mantione, I. del Agua, A. Sanchez-Sanchez and D. Mecerreyes, *Polymers (Basel).*, 2017, 9.

16 T. Galán, B. Prieto-Simón, M. Alvira, R. Eritja, G. Götz, P. Bäuerle and J. Samitier, *Biosens. Bioelectron.*, 2015, **74**, 751–756.

17 G. Dufil, D. Parker, J. Y. Gerasimov, T. Q. Nguyen, M. Berggren and E. Stavrinidou, *J. Mater. Chem. B*, 2020, **8**, 4221–4227.

18 D. Mantione, , E. Istif, G. Dufil, L. Vallan, D. Parker, C. Brochon, E. Cloutet, G. Hadziioannou, M. Berggren, E. Stavrinidou and E. Pavlopoulou, *ACS Appl. Electron. Mater.*, 2020, **2**, 4065–4071.

19 S. H. Su, N. M. Gibbs, A. L. Jancewicz and P. H. Masson, *Curr. Biol.*, 2017, 27, R964–R972.

20 B. K. Ham, J. Chen, Y. Yan and W. J. Lucas, *Curr. Opin. Biotechnol.*, 2018, 49, 1–9.

21 J. Lamers, T. Van Der Meer and C. Testerink, *Plant Physiol.*, 2020, **182**, 1624–1635.

22 S. A. Rolfe, J. Griffiths and J. Ton, *Curr. Opin. Microbiol.*, 2019, 49, 73–82.

23 A. V. Volkov, K. Wijeratne, E. Mitraka, U. Ail, D. Zhao, K. Tybrandt, J. W. Andreasen, M. Berggren, X. Crispin and I. V. Zozoulenko, *Adv. Funct. Mater.*, , DOI:10.1002/adfm.201700329.

24 V. B. Ivanov and J. G. Dubrovsky, *Trends Plant Sci.*, 2013, 18, 237–243.

25 A. Barrada, M. H. Montané, C. Robaglia and B. Menand, *Int. J. Mol. Sci.*, 2015, 16, 19671–19697.

26 R. De-Jesús-García, U. Rosas and J. G. Dubrovsky, *Funct. Plant Biol.*, 2020, 47, 383–397.

27 J. Namyslov, Z. Bauriedlová, J. Janoušková, A. Soukup and E. Tylová, *Plants*, , DOI:10.3390/plants9020201.

28 A. Berhin, D. de Bellis, R. B. Franke, R. A. Buono, M. K. Nowack and C. Nawrath, *Cell*, 2019, **176**, 1367-1378.e8.

29 R. P. Kumpf and M. K. Nowack, *J. Exp. Bot.*, 2015, 66, 5651–5662.

30 P. W. Barlow, *J. Plant Growth Regul.*, 2002, 21, 261–286.

31 C. Durand, M. Vicré-Gibouin, M. L. Follet-Gueye, L. Duponchel, M. Moreau, P. Lerouge and A. Driouich, *Plant Physiol.*, 2009, **150**, 1411–1421.

32 M. Cai, N. Wang, C. Xing, F. Wang, K. Wu and X. Du, *Environ. Sci. Pollut. Res.*, 2013, **20**, 8924–8933.

33 N. Kumar and A. S. Iyer-Pascuzzi, *Plants*, 2020, 9.

34 G. Dijk, A. L. Rutz and G. G. Malliaras, *Adv. Mater. Technol.*, , DOI:10.1002/admt.201900662.

35 A. D. French, *Cellulose*, 2014, **21**, 885–896.

36 K. E. Aasmundtveit, E. J. Samuelsen, L. A. A. Pettersson, O. Inganäs, T. Johansson and R. Feidenhans'l, *Synth. Met.*, 1999, **101**, 561–564.

37 J. F. Franco-Gonzalez, E. Pavlopoulou, E. Stavrinidou, R. Gabrielsson, D. T. Simon, M. Berggren and I. V. Zozoulenko, *Nanoscale*, 2017, **9**, 13717–13724.

38 A. V. Volkov, S. K. Singh, E. Stavrinidou, R. Gabrielsson, J. F. Franco-Gonzalez, A. Cruce, W. M. Chen, D. T. Simon, M. Berggren and I. V. Zozoulenko, *Adv. Electron. Mater.*, , DOI:10.1002/aelm.201700096.

39 K. Tybrandt, I. V. Zozoulenko and M. Berggren, *Sci. Adv.*, , DOI:10.1126/sciadv.aao3659.

40 A. Malti, J. Edberg, H. Granberg, Z. U. Khan, J. W. Andreasen, X. Liu, D. Zhao, H. Zhang, Y. Yao, J. W. Brill, I. Engquist, M. Fahlman, L. Wågberg, X. Crispin and M. Berggren, *Adv. Sci.*, , DOI:10.1002/advs.201500305.

41 M. G. Say, R. Brooke, J. Edberg, A. Grimoldi, D. Belaineh, I. Engquist and M. Berggren, *npj Flex. Electron.*, , DOI:10.1038/s41528-020-0079-8.

42 H. Wang, Y. Diao, Y. Lu, H. Yang, Q. Zhou, K. Chrulski and J. M. D'Arcy, *Nat. Commun.*, , DOI:10.1038/s41467-020-17708-1.

43 R. Reece, C. Lekakou and P. A. Smith, *ACS Appl. Mater. Interfaces*, 2020, **12**, 25683–25692.

44 M. O. Bamgbopa, D. Belaineh, D. A. Mengistie, J. Edberg, I. Engquist, M. Berggren and K. Tybrandt, *J. Mater. Chem. A*, 2021, **9**, 2184–2194.

45 P. Tripathi, S. Subedi, A. L. Khan, Y.-S. Chung and Y. Kim, *Plants*, 2021, **10**, 885.

46 G. Guerriero, J. F. Hausman and S. Legay, *Front. Plant Sci.*, 2016, 7.